Journal of Medicinal Chemistry Article

J. Med. Chem. **2009,** *52,* 7069–7080 **7069**
DOI: 10.1021/jm900969p

Inhibitors for Human Glutaminyl Cyclase by Structure Based Design and Bioisosteric Replacement

Mirko Buchholz,[†] Antje Hamann,[†] Susanne Aust,[†] Wolfgang Brandt,[§] Livia Böhme,[∞] Torsten Hoffmann,[∞] Stephan Schilling,[‡] Hans-Ulrich Demuth,[†,‡,∞] and Ulrich Heiser*,[†]

[†]*Department of Medicinal Chemistry and* [‡]*Department of Enzymology and* [∞]*Department of Preclinical Pharmacology, Probiodrug AG, Weinbergweg 22, 06120 Halle, Germany, and* [§]*Department of Bioorganic Chemistry, Leibniz Institute of Plant Biochemistry, Weinberg 3, D-06120 Halle, Germany*

Received July 1, 2009

The inhibition of human glutaminyl cyclase (hQC) has come into focus as a new potential approach for the treatment of Alzheimer's disease. The hallmark of this principle is the prevention of the formation of $A\beta_{3,11(pE)-40,42}$, as these Aβ-species were shown to be of elevated neurotoxicity and likely to act as a seeding core leading to an accelerated formation of Aβ-oligomers and fibrils. Starting from 1-(3-(1*H*-imidazol-1-yl)propyl)-3-(3,4-dimethoxyphenyl)thiourea, bioisosteric replacements led to the development of new classes of inhibitors. The optimization of the metal-binding group was achieved by homology modeling and afforded a first insight into the probable binding mode of the inhibitors in the hQC active site. The efficacy assessment of the hQC inhibitors was performed in cell culture, directly monitoring the inhibition of $A\beta_{3,11(pE)-40,42}$ formation.

Introduction

The N-terminal modification of peptides by the generation of a pGlu[a] moiety from the corresponding glutamine precursors is an important process in the maturation of bioactive peptides[1−3] which is catalyzed by glutaminyl cyclases (QC).[4] QC activity is commonly found in nature.[5−8] In the case of the mammalian QC activity, the catalytic process is found to be zinc-dependent[9] whereas bacterial and plant QC catalysis differs with regard to mechanism and the structure of the catalyzing protein.[10,11] The protein structure of human QC is closely related to bacterial aminopeptidases and other members of the zinc hydrolase family.[12,13] In contrast to structurally related aminopeptidases, mammalian QCs possess only one zinc ion in the active site adopting a tetrahedral geometry.[9,13,14]

The protein sequence is highly conserved throughout the different mammalian species, thereby having an identity of 80−90%.[15] The recently identified isoforms of the human and murine enzymes have a high sequence homology and show a close substrate specificity compared to the human protein.[16]

Human QC activity is highly abundant in secretory and neuronal tissue;[17] it is preferentially found in brain regions such as hippocampus and hypothalamus.[7,17] Recent developments have related QC activity to the processing of the β-amyloid peptides (Aβ) in the course of Alzheimer's disease (AD).[18−20] It was shown that QC is probably the responsible enzyme for the formation of N-terminal pGlu residues after the liberation of the N-terminus of glutamate at position 3 of the Aβ-peptide, thereby exhibiting a glutamate cyclase (EC) activity.[21] The formation of this modified Aβ species is likely to be a crucial event in the initiation and the progress of the disease, as these pGlu containing peptides exhibit an elevated neurotoxicity and a tendency to aggregate.[22−24]

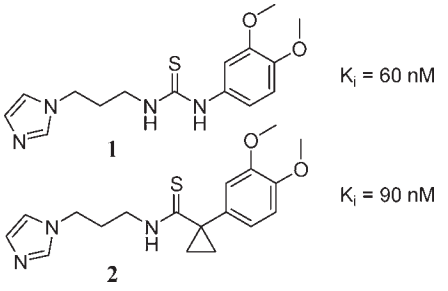

Figure 1. First potent hQC inhibitors.[26]

The application of inhibitors of QC as a new strategy for the treatment of AD has proven to be successful in different transgenic animal models.[19,25] A reduction of the amount of pGlu peptides as well as the total plaque load was achieved, leading to a significant improvement of learning and memory.[19]

Recently, we have presented the first generation of potent QC inhibitors (Figure 1).[26] The compounds were developed without information of the target protein structure, postulating the contact of the *N*-alkylimidazole with the catalytic zinc ion to be crucial for the inhibitory potency.

In this manuscript we describe further development of QC inhibitors by means of a structure-based approach utilizing a homology model of the enzyme. Furthermore, new active compound classes could be identified by the bioisosteric replacement of the unfavorable thiourea moiety.[27−31] The efficacy of the compounds regarding their ability to suppress pGlu formation at the N-terminus of the Aβ-peptide was shown in a cell-based model.

*To whom correspondence should be addressed. Phone: +49 (0) 345 5559908. Fax: +49 (0) 345 5559901. E-mail: ulrich.heiser@probiodrug.de.

[a]Abbreviations: hQC, human glutaminyl cyclase; pGlu, pyro-glutamyl.

Published on Web 10/28/2009

Scheme 1[a]

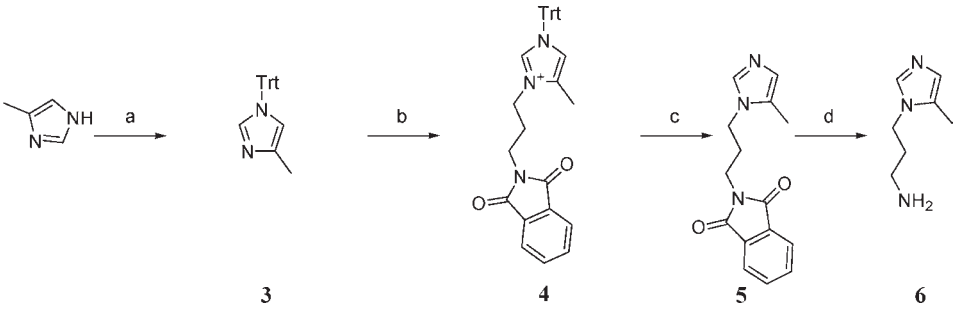

[a] Reagents and conditions: (a) trityl chloride, NEt_3, DMF, 12 h, room temp; (b) 2-(3-bromopropyl)isoindoline-1,3-dione, MeCN, 12 h, reflux; (c) TFA (5%), MeOH, 3 h, reflux; (d) hydrazine, EtOH, 8 h, reflux, then 4 N HCl, 4 h, reflux.

Scheme 2[a]

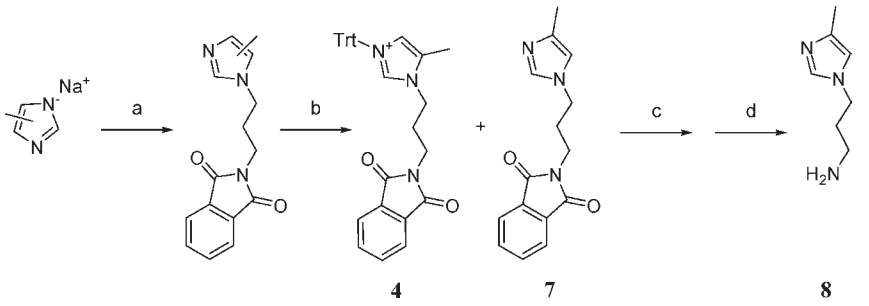

[a] Reagents and conditions: (a) 2-(3-bromopropyl)isoindoline-1,3-dione, DMF, 8 h, 90 °C; (b) trityl chloride, dichloromethane, 1.5 h 0 °C to room temp; (c) chromatographic separation; (d) **7**, hydrazine, EtOH, 8 h, reflux, then 4 N HCl, 4 h, reflux.

Results and Discussion

Chemistry. The methylaminopropylimidazole precursors were synthesized starting from 4-methylimidazole via a modified Gabriel synthesis,[26] whereas a regioselective alkylation route was applied in order to yield the respective methyl substituted derivatives **6** and **8**.

In the case of the 5-methyl derivative **6**, 4-methyl-1-*H*-imidazol was reacted with trityl chloride and triethylamine according to Scheme 1, yielding 1-trityl-4-methylimidazole (**3**) exclusively. After quaternation the resulting 1-trityl-3-[3-(1,3-dioxo-1,3-dihydro-2*H*-isoindol-2-yl)propyl]-4-methyl-1*H*-imidazol-3-ium chloride **4** was deprotected yielding **5**. The subsequent hydrazinolysis led to the 3-(5-methyl-1*H*-imidazol-1-yl)propyl-1-amine **6**.

The synthesis of 4-methyl derivative **8** (Scheme 2) started with the alkylation of sodium 4-methyl-1*H*-imidazolate with 2-(3-bromopropyl)isoindolin-1,3-dione. The resulting mixture of 2-(3-(5-methyl-1*H*-imidazol-1-yl)propyl)isoindoline-1,3-dione and 2-(3-(4-methyl-1*H*-imidazol-1-yl)propyl)isoindoline-1,3-dione was reacted with trityl chloride, leading to a quaternation product only in the case of the 2-(3-(5-methyl-1*H*-imidazol-1-yl)propyl)isoindoline-1,3-dione (**4**). The quaternized species could be separated by means of flash chromatography, yielding 2-(3-(4-methyl-1*H*-imidazol-1-yl)propyl)isoindoline-1,3-dione (**7**), which was then converted into 3-(4-methyl-1*H*-imidazol-1-yl)propyl-1-amine (**8**) by hydrazinolysis.

The preparation of the thiourea (**9** and **10**) and the thioamide (**11** and **12**) derivatives was accomplished according to Scheme 3.[26] The cyanoguanidine derivatives (**13**−**21**, **36**−**40**, and **51**) were prepared according to Scheme 4.[32] Sodium cyanamide and the respective isothiocyanate were reacted leading to a thiourea intermediate. The respective 1-alkylimidazol moiety was introduced by means of water-soluble carbodiimide (WSCD). The nitrovinyldiamines (**22**−**30**, **41**−**45**, and **52**) were obtained by a stepwise reaction of 2,2-bis-methylthio-1-nitroethene with the corresponding amines (Scheme 5).[33] The synthesis of the 2-thioxopyrimidin-4(1*H*)-ones (**31**−**35**, **46**−**50**, and **53**) was accomplished via the corresponding (5-alkyloxycarbonyl)arylthiourea derivatives by the formation of an amide bond leading to a ring closure at the 1-nitrogen of the thiourea moiety (Scheme 6).

Structure−Activity Relationship. The cyanoguanidines **13**−**21** (Table 1) were found to be of medium potency. Compounds containing alkyl substituents like methyl (**13**) and cyclopropylmethyl (**14**) exhibited a potency comparable to that of phenyl (**15**), 4-bromophenyl (**16**), and 3,4-dimethoxyphenyl (**20**) derivatives. A 6-fold decrease was found for the 4-trifluormethylphenyl derived inhibitor **17**. In contrast to that, the 4-isopropylphenyl- (**18**), the 4-methoxyphenyl (**19**), and the tethering of the 3- and 4-methoxy substituent as in (**21**) had a slightly improved potency.

The influence of the variable substituent was found to be more pronounced in the case of the nitrovinyldiamine derivatives (Table 1). In this case, the methyl derivative **22** was found to be inactive. The compounds with aromatic substituents (**24**−**27**, **29**, and **30**) were of comparable potency with exceptions found in the plain phenylnitrovinyldiamine (**24**) and 4-methoxynitrovinyldiamine (**28**), which were found to be less active. The character of the para-substituent at the phenyl ring was of low influence in this group of compounds, as the 4-chloronitrovinyldiamine and the 4-trifluormethylphenylnitrovinyldiamine had comparable inhibitory potency. Surprisingly **23**, containing cyclohexyl substituents, was found to be as active as the phenyl derivatives **24**−**27**, **29**, and **30**.

When the classes of the cyanoguanidines and nitrovinyldiamines are compared, major differences are found with the

Scheme 3[a]

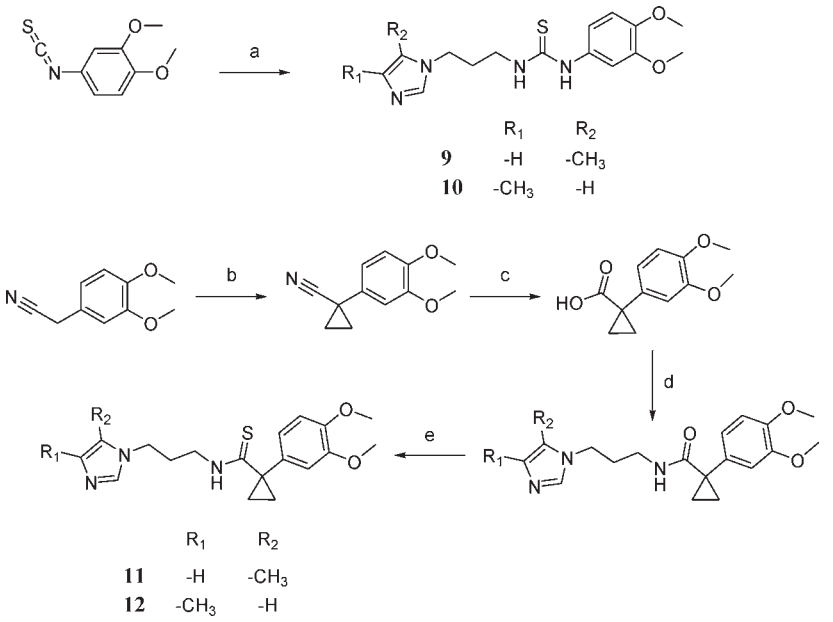

[a] Reagents and conditions: (a) **6** or **8**, EtOH, 2 h, reflux; (b) 1-bromo-2-chloroethane, TEBA, KOH, 2 d, room temp; (c) KOH, ethylene glycol, 12 h, reflux; (d) **6** or **8**, CAIBE, NMM, THF, 5 min, −5 °C, 10 h, room temp; (e) Laweson′s reagent, 1,4-dioxane, 8 h, reflux.

Scheme 4[a]

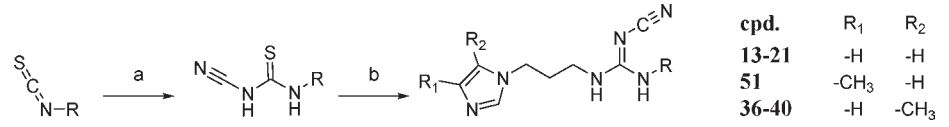

[a] Reagents and conditions: (a) potassium cyanamide, EtOH, 2 h, reflux; (b) 3-(1*H*-imidazol-1-yl)propan-1-amine, **6** or **8**, WSCD, DMF−EtOH, 2 h, room temp.

Scheme 5[a]

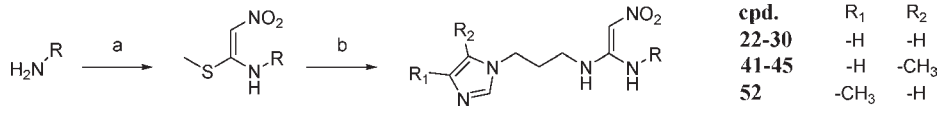

[a] Reagents and conditions: (a) 1,1-bis(methylthio)-2-nitroethene, EtOH, 24 h, reflux; (b) 3-(1*H*-imidazol-1-yl)propan-1-amine, **6** or **8**, EtOH, 24 h, reflux.

Scheme 6[a]

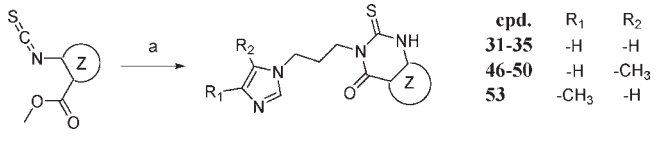

[a] Reagents and conditions: (a) 3-(1*H*-imidazol-1-yl)propan-1-amine, **6** or **8**, EtOH, 2 h, reflux.

alkyl-type derivatives **13**, **14**, **22**, and **23** with a preference for the methyl substitution in the case of the cyanoguanidines (**13**) and the cyclohexyl substitution in the case of the nitrovinyldiamines (**23**). The trifluoromethylphenyl substituent, as in **17** and **26**, having a lower electron density in the aromatic ring, led to more active inhibitors when incorporated in a nitrovinyldiamine such as in **26**. The 4-methoxyphenyl substitution was better accepted in cyanoguanidines (**19**), whereas the 3,4-dimethoxyphenyl nitrovinyldiamine inhibitor **29** was found to be more potent as the corresponding cyanoguanidine equivalent **21**.

The incorporation of the known thiourea motif[26] into a condensed ring system as thioxopyrimidine led to potent compounds. Only little differences in the potency between the derivatives were seen, depending on the ring size and the character of the condensed ring (Table 2). The phenylthiophene (**31**) and the 3-methylthiophene derivative (**32**) as well as the 2,3-dihydrobenzo[*b*][1,4]dioxin containing compound (**33**) were of comparable potency. Only a little decrease of the potency was observed in the case of an extension or reduction of the attached saturated ring (**34**, **35**).

The introduction of a methyl group in position 4 of the imidazole did not affect the inhibitory potency compared to the nonsubstituted equivalents. This finding holds true for all examples of the molecular scaffolds investigated (Tables 2 and 3). Only a slight improvement by 2-fold was visible in the case of the thioamide **12** in comparison to the nonmethylated analogue **2**. In the case of the cyanoguanidine example **51** and the nitrovinyldiamine **52** the activity dropped by a factor of 2.5 compared to the unsubstituted derivatives **21** and **30**.

Table 1

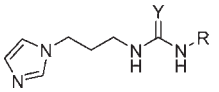

cpd	Y	R	K_i [nM]	cpd	Y	R	K_i [nM]
13	-N-CN	-CH_3	1530 ± 50	**22**	-CH-NO_2	-CH_3	20550 ± 680
14	-N-CN		1370 ± 30	**23**	-CH-NO_2		500 ± 30
15	-N-CN		1020 ± 20	**24**	-CH-NO_2		1170 ± 70
16	-N-CN	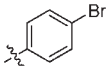	1090 ± 70	**25**	-CH-NO_2	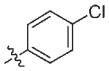	570 ± 30
17	-N-CN	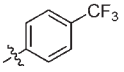	6720 ± 150	**26**	-CH-NO_2	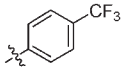	540 ± 40
18	-N-CN	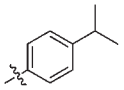	830 ± 20	**27**	-CH-NO_2	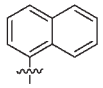	520 ± 20
19	-N-CN	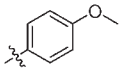	700 ± 10	**28**	-CH-NO_2	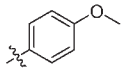	1030 ± 70
20	-N-CN	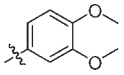	1360 ± 60	**29**	-CH-NO_2	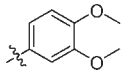	610 ± 60
21	-N-CN	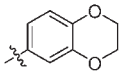	620 ± 60	**30**	-CH-NO_2	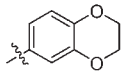	540 ± 40

A general improvement of the inhibitory potency was observed when the methyl substitution was introduced at position 5 of the imidazole ring (Table 4). An elevation of 10-fold was shown for the thiourea **9** in comparison to **1** and **10**, up to 15-fold in the case of the thioamides **11** and **12**, or even 35-fold as for **11** and **2**. The cyanoguanidine **39** was found to be 5-fold more active as the unsubstituted **21** and 13-fold more active as the 4-methylimidazole **51**. A comparable result was found for the nitrovinyldiamines with a 8.1-fold improvement in the case of **30** compared to **45** and a 19-fold improvement for **52** compared to **45**.

A similar result was found for the of 2-thioxopyrimidin-4(1*H*)one class (Table 2). The 5-methylation as in **46** led to an improvement of the activity by a factor of 17 in comparison to **31** and a factor of 13 in comparison to **53**, respectively.

The SAR investigation of 5-methyl-1*H*-imidazol-1-yl)propylamino inhibitors (Table 4) of the cyanoguanidine and nitrovinyldiamine type features most of the compounds with a QC inhibitory activity in the low nanomolar range, where the differences in the activity of the compounds are found to be low. In the case of the cyanoguanidines, the activity difference between the most active compound **40** and the most inactive compound **37** is only 4-fold. Therefore, a 3,4-dimethylphenyl moiety (**36**) is as well tolerated as a biphenyl (**38**) or a 3,4,5-trimethoxyphenyl substituent (**40**). A slightly decreased activity was observed when the 3,4-dimethylphenyl in **36** was exchanged by a dioxine as in **39** or a 3,4-dichlorophenyl as in **37**. For the nitrovinyldiamines the activity range was found to be even smaller with a 2-fold difference between **45** as the most inactive compound and **43** as the most active inhibitor of this class. Therefore, the character of the substituent had no major influence on the inhibitory potency. For example, a compound containing a cyclohexyl moiety (**41**) was found to be as potent as a *p*-chlorophenyl- (**42**), a *p*-trifluoromethylphenyl- (**43**), an α-naphtyl- (**44**), or even a 2,3-dihydrobenzo[*b*][1,4]dioxine bearing substituents (**45**).

The class of the 5-methylimidazolpropyl-2-thioxopyrimidin-4(1*H*)-ones (Table 2) showed an activity range that is comparable to that of the corresponding cyanoguanidines (Table 4) with a factor of 5 between **50** and **47**. For this class a 2,3-dihydro-2-thioxoquinazolin-4(1*H*)-one as in **46** was spatially extendable by a 2-thioxo-2,3,5,6,7,8-hexahydro[1]-benzothieno[2,3-*d*]pyrimidin-4(1*H*)-one as in **47**, retaining the inhibitory potency. The extension of the cyclohexyl moiety of **47** into a cyclooctyl group as in **48** caused a slight loss of activity. When the thieno part was substituted with a benzyl moiety at position 6 as in **49**, no influence on the activity is detectable in comparison to the unsubstituted analogues **46** and **47**. However, the substitution at the 5-position with a phenyl ring in **50** led to a slight loss of activity by a factor of around 5 compared to **47** and **49**.

Table 2

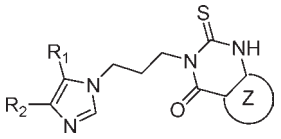

compound	R_1	R_2	Z	K_i [nM]
31	H	H		300 ± 3
32	H	H		360 ± 3
33	H	H		340 ± 6
34	H	H		620 ± 20
35	H	H		900 ± 30
53	H	CH_3		230 ± 6
46	CH_3	H		18 ± 1.9
47	CH_3	H	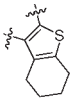	17 ± 0.3
48	CH_3	H	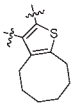	39 ± 1.0
49	CH_3	H	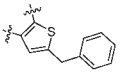	20 ± 0.6
50	CH_3	H	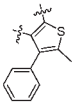	83 ± 3.0

Biology. The assessment for the efficacy of the different hQC inhibitors was performed in a cell culture assay using transfected HEK293 cells expressing human APP and hQC. The APP expression construct featured a deletion of the first two amino acids of the Aβ sequence leading to the direct liberation of $A\beta_{3\text{-}40,42}$ by β- and γ-secretase activity.[34] The cotransfection with hQC caused the production of $A\beta_{3(pE)\text{-}40,42}$ in amounts of 5−20% of the total $A\beta_{x\text{-}40,42}$ as quantified by an ELISA assay applying N-terminal specific antibodies.[35] In this setting, the effective hQC inhibitor **1** (PBD150)[26,35] led to a 70% reduction of $A\beta_{3(pE)\text{-}40,42}$ in relation to the untreated controls, and therefore, **1** was used as a benchmark for the assessment of the current inhibitors. A total of 23 compounds was assessed regarding their

Table 3

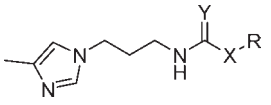

cpd	X	Y	R	K_i [nM]
10	-NH-	S	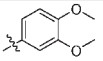	60 ± 1.0
12		S	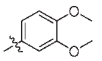	41 ± 2.0
51	-NH-	-N-CN	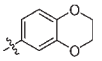	1650 ± 60
52	-NH-	-CH-NO_2	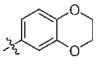	1290 ± 73

efficacy in the inhibition of A$\beta_{3(pE)-40,42}$ formation on transfected HEK cells. Taking **1** as the benchmark for the potency in hQC inhibition, the selection included hQC inhibitors regarded as potent, such as **2**, **9**, **11**, **46**, **47**, and **49**, medium potent such as **10**, **33**, **36**, **38**, **39**, **40**, **41**, **42**, **45**, and **53**, and low potent inhibitors such as **51**, **52**, and **53**. As a result, the potency of the compounds at the isolated target was reflected by the efficacy inhibiting the formation of pGlu containing Aβ-peptides in general (Figure 2). The most potent hQC inhibitors **2**, **9**, **11**, **46**, **47**, and **49** inhibited the formation of A$\beta_{3(pE)-40,42}$ with an efficacy above 90% using the concentrations indicated. Compounds with a medium inhibitory potency such as **10**, **33**, **36**, **38**, **39**, **40**, **41**, **42**, **45**, and **53** were found to be able to prevent the formation of A$\beta_{3(pE)-40,42}$ by 30−70%, not generally paralleling their potency found during hQC inhibition in vitro. For less potent compounds such as **51**, **52**, and **53**, a K_i value on hQC above 1 μM was revealed to be not effective in reducing the A$\beta_{3(pE)-40,42}$ formation. The most effective compound **47** led to a total blockage of the A$\beta_{3(pE)-40,42}$ formation at 1 μM.

Computational Chemistry

hQC Homology Model. The homology model of hQC was developed using the X-ray structures of the aminopeptidase from *Aeromonas proteolytica* (apAP, PDB codes 1amp and 1rtq) and a hQC model (PDB code 1moi)[12] lacking the information regarding the catalytic zinc ion. After the superimposition[36] of the active sites of 1rtq and 1moi the catalytic zinc ion (Zinc 1) with the attached water molecule was transferred to the homology model 1moi. The template aminopeptidase contains two catalytic zinc ions (Zinc 1 and Zinc 2). It was previously shown that the hQC protein contains only one active zinc ion,[9,37] a fact that is meanwhile proven by the solution of the hQC protein structure.[13] In the case of the hQC homology model it was postulated that the Zinc 1 of the aminopeptidase corresponds to the zinc ion found in hQC, as for this position a greater zinc affinity over position 2 is described.[38,39] The template topology of 1rtq on the loop region between T222 and S228 led to an unfavorable superimposition of the side chain of the residue Q304 of hQC (1moi) to the side chain from C237 of apAP (1rtq). In this conformation the access to the active site was blocked by the side chain of Q304, making the binding of the known inhibitor structures unlikely. An explanation was found in the presence of a disulfide bridge between the C223 and C227 in the structure of the aminopeptidase template, which is lacking the hQC protein. For that reason the side chain of Q304 was turned manually followed by a molecular dynamic simulation of the whole loop. The hQC model (Figure 3) reveals the typical "open sandwich" structure adopted from the aminopeptidase template. The structural topology with a hydrophobic core consisting of four parallel and two antiparallel β-sheets and the surrounding eight α-helices represents the typical α/β-hydrolase fold. When the homology model of hQC and the template aminopeptidase are compared, a high similarity was found not only for the overall structure but also for zinc binding site and for most of the active site amino acid residues as represented by the rmsd values (Figure 3). Structural differences, resulting in higher rmsd values, were found in the loop region (S288−D305), which was modified by MD simulation. Further differences were visible at the position of W329 in the hQC model that lacks an equivalent in the apAP structure. Other differences between the template and the model were found in areas away from the active site at the loops K176−S187 and F204−D211.

The active site is characterized by a deep, tight, and angled cleft, which is defined by the hydrophobic amino acids W329, V302, D305 (not shown). This cleft opens in a bigger cavity of about 8 Å × 8 Å × 10 Å defined by the distances between the zinc ion and the atom OD1 of D248, the atom CD1 of L249 and atom OD2 of D305, and between the atom NE2 of H140 and atom OH of Y299, respectively. The zinc ion, located at the bottom of this cavity, is coordinated by H330, E202, D159, and the imidazole moiety of the inhibitor (Figures 3 and 4). A stepwise strategy was applied for the shaping of the active site of the homology model using the different known inhibitor structures *N*-methyl imidazole,[9] *N*-benzylimidazole,[9] and compound **1**. After each step a MD simulation was performed, keeping only the amino acids in a range of 4.5 Å around the respective inhibitor flexible. In the first step the N3 of 1-methylimidazole was placed on the free coordination site adopted by the coordinating water in the case of the free enzyme. After the MD simulation the same procedure was repeated with *N*-benzyl-imidazole and compound **1**, respectively. The resulting model was then visually inspected, and the amino acids that were identified to have geometry failures according to the Ramachandran plot were adjusted stepwise followed by energy minimization steps. The 3,4-dimethoxyphenyl moiety of compound **1** was found to be localized at a region, which is formed by the hydrophobic side chains of the residues Y299, F325, P326 and the acidic side chain of E327. This area corresponds to the positions of F244, Y248, and Y251 in apAP, which are involved in forming a hydrophobic pocket discussed to be the S1-recognition site of aminopeptidases (Figure 3).[40]

Docking. The binding pose of the imidazole part of **1** resulting from the MD simulation was used as a substructure constraint for the docking[41] of the inhibitory molecules **1**, **2**, and **9**−**12**. The resulting poses were scored applying the ChemScore function containing an explicit metal binding term. The visual inspection of the docking results of **1** and **2** suggested an open space between the imidazole and the active site in the near of the carbon 5, which could be filled by additional substituents. In contrast to that, the space surrounding the carbon 4 appeared to be smaller (Figure 4). Supporting this finding, the solutions of the scoring function for the thiourea derivatives **1**, **9**, and **10** showed a preference of the 5-methyl compound **9** over the nonsubstituted derivative **1** and the 4-methylated **10**. The 5-methyl derivative **11** again was found to have the highest score, followed by the unsubstituted imidazole derivative **2** and the corresponding 4-methyl compound **12**. The low score for the 4-methyl derivatives was mainly caused by a high contribution of the clash-term to the lower scoring value (Supporting Information).[41]

Discussion

The bioisosteric replacement of the thiourea moiety by cyanoguanidines and nitrovinyldiamines starting from **1** led

Table 4

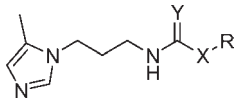

compound	X	Y	R	K_i [nM]
9	NH	S	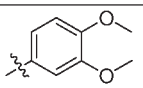	6.3 ± 0.45
11	S		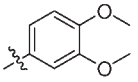	2.6 ± 0.08
36	NH	-N-CN	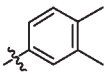	82 ± 8.5
37	NH	-N-CN	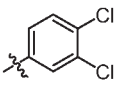	253 ± 6
38	NH	-N-CN	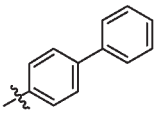	65 ± 3.1
39	NH	-N-CN	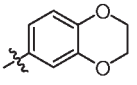	130 ± 6
40	NH	-N-CN	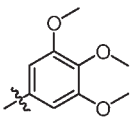	61 ± 3.1
41	NH	-CH-NO_2		44 ± 4.1
42	NH	-CH-NO_2	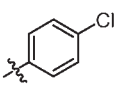	51 ± 4.6
43	NH	-CH-NO_2	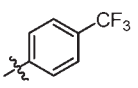	34 ± 3.0
44	NH	-CH-NO_2	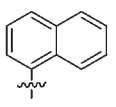	42 ± 1.4
45	NH	-CH-NO_2	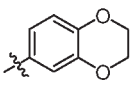	67 ± 6.5

to compounds with a QC inhibiting potency in the submicromolar range. The most potent compounds, **21** for the cyanoguanidines and **23** for the nitrovinyldiamines, were found to be 10-fold less potent than the active compound **1**, belonging to the thiourea class. In general, the SAR within the classes of investigated compounds lacks deep activity clefts. An unexpected observation was made within the class of the nitrovinyldiamines, wherein saturated carbocyclic substituents as in **23** were found to be more potent as the corresponding phenyl derivative **24**. This finding stands in contrast to the SAR of the thioureas, where the cyclohexyl substituted thiourea derivative was found to be of equal potency as the respective phenyl derivative.[26] Differences in the SAR are visible when comparing similar molecules belonging to different classes. The methylcyanoguanidine **13** is 13-fold more active than the corresponding nitrovinyldiamine **22**; in contrast to this the

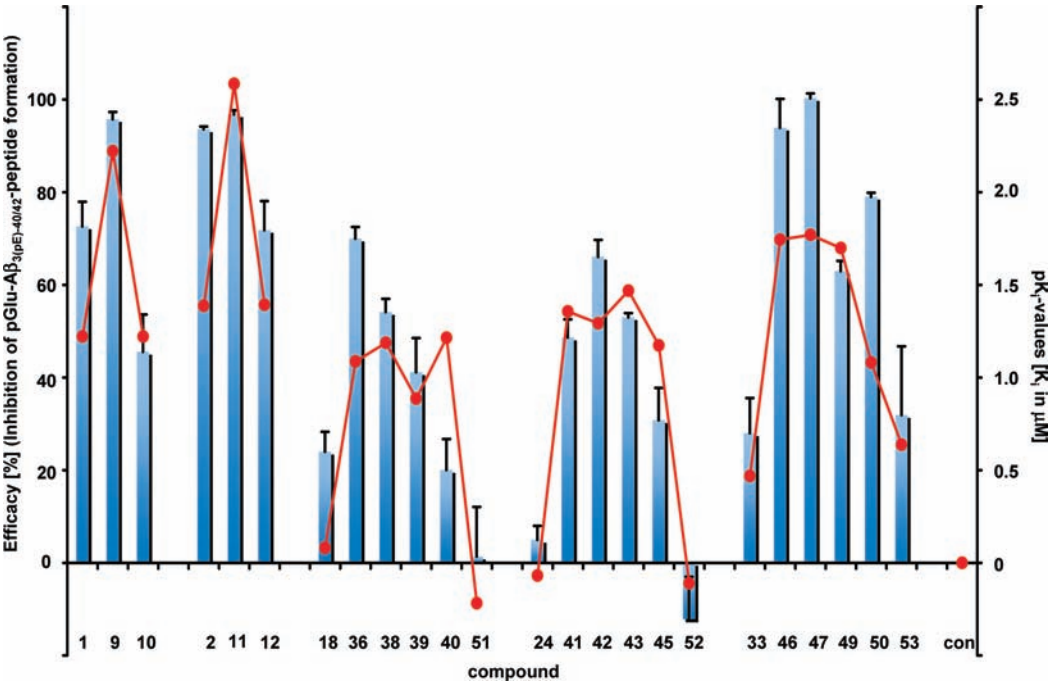

Figure 2. Efficacy (% of inhibition of pGlu-A$\beta_{3(pE)-40/43}$ formation, blue bars) of selected hQC inhibitors (1 μM) in hQC and NLE overexpressing HEK cells compared with their hQC inhibitory potency (pK_i, red dots).

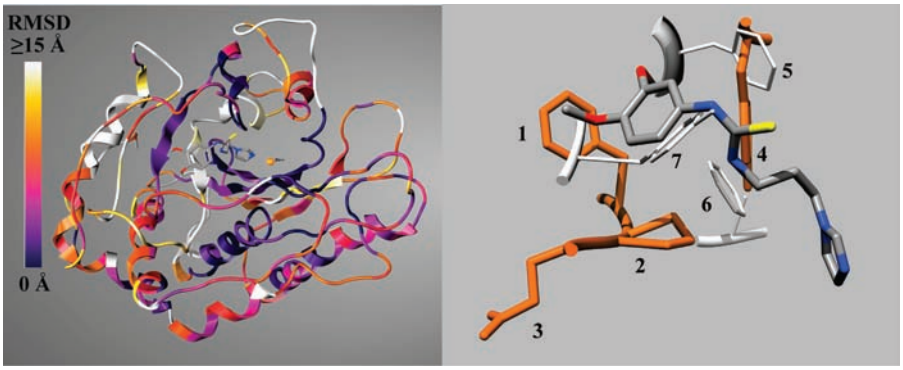

Figure 3. Left: Homology model of hQC. The colors correspond to rmsd values between the mass centers of the amino acids after structural alignment with the aminopeptidase template 1amp. The binding pose of **1** after MD simulation is shown. Right: Possible binding mode of **1** at a hydrophobic area formed by the amino acid residues: (1) F325, (2) P326, (3) E327, and (4) Y299 (orange) in the homology model. For comparison prominent amino acids of the hydrophobic S1 pocket of apAP (1amp) are shown in white: (5) F248, (6) F244, and (7) Y251.

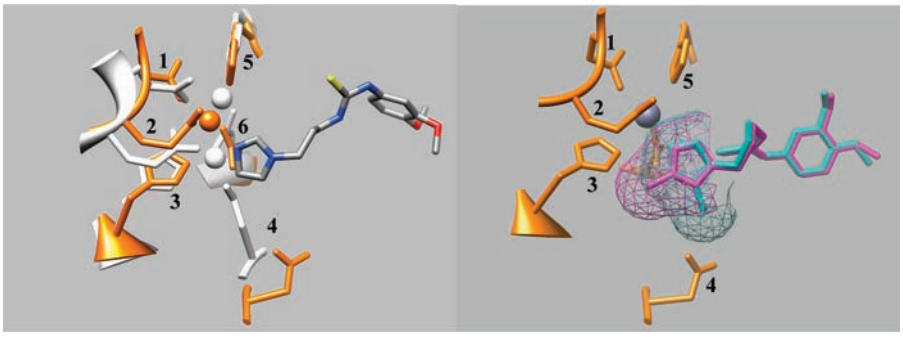

Figure 4. Left: Position of **1** after MD simulation. Shown are the residues of the metal-binding site and the catalytic zinc ion of the hQC homology model (orange). The metal-binding site of apAP (white) bearing two zinc ions is shown for comparison. Right: Docking of **9** (pink) and **10** (blue) in the active site. The van der Waals surfaces of the imidazoles are visualized. Amino acids (hQC/apAP) are as follows: (1) E201/151, (2) E202/152, (3) H140/97, (4) D248/179, (5) H330/266, and (6) D159/117.

corresponding phenyl derivatives **15** and **24** display the same potency. A possible explanation for this could be found in the different binding mode of the respective methyl derivatives **13** and **22**. In this case, the cyano part of **13** could adopt the same hydrophobic interaction with the protein as the phenyl part of **15**. This assumption is supported by the results of docking

investigations (not shown) and the bioisosteric replacement of phenyl groups by cyano moieties, which is established to be possible.[28,29]

2-Thioxopyrimidin-4(1*H*)ones were identified as potent compounds in general, exhibiting inhibitory activities in the lower micromolar range. For the investigated compounds only little differences in the inhibitory potency were recognizable, depending on the size of the annulated saturated ring (see compounds **33**, **34**, and **35**).

The optimized potency of the 5-methylimidazole thiourea was found to be consistent within the bioisosteric cyanoguanidines, nitrovinyldiamines, and the 2-thioxopyrimidin-4-(1*H*)ones. The gain of potency ranges between a factor of 13 and 20, by comparing the 4-methyl derivatives with the respective 5-methylimidazoles. This corresponds to an average gain of free binding energy of 1.57 ± 0.15 kcal/mol comparing all 5-methyl derivatives with their corresponding 4-methyl analogues.[42] The differences of the inhibitory potency among the different 5-methylimidazoles were low. This leads to the assumption that the effective binding of the 5-methylimidazoles as metal binding group overrules the contribution of the different remaining parts of the inhibitor molecules. **11** with a K_i value of 2.6 nM is the most potent inhibitor of hQC described so far. A reason for the generally elevated efficacy of the 5-methylimidazoles could be found in an optimized binding due to sterical conditions as well as the improvement of the metal binding properties of the imidazole N3-nitrogen. The first hint supporting this hypothesis could be the shift of the calculated pK_a[43] of the imidazole N3-nitrogen from 6.79 for **1** and 6.65 for **10** toward 7.33 for **9** pointing toward a better metal binding with a more basic, electron rich coordination site.

The first insight into the possible binding mode of hQC inhibitors gained by the development of a homology model partly reflected the findings from the structure−activity relationship studies of hQC inhibitors. Provided that the imidazole acts as the metal-binding group via its N3-nitrogen, the length of the spacer between the imidazole and the molecular scaffold was optimal when consisting of three methylene units. A shorter linker, like ethyl, would cause a steric clash with the tight cleft formed by the amino acids W329, V302, and Y299 (not shown). This result is in accordance with previous findings, wherein the ethyl derivative of **1** is 300-fold less active.[26] The thiourea motif with its ability to flip the thio amide bond enables a possible interaction of the 3,4-dimethoxyphenyl moiety of the inhibitor with a pocket of the enzyme formed by the side chains of the residues Y299, F325, P326, and E327. The second zinc ion lacking in the hQC protein, but present in the aminopeptidase template, leaves a space that can be filled by substituents located at position 5 of the metal-interacting imidazole ring of the inhibitor. As this area of the active site is highly conserved in the hQC sequence, the resulting homology model has a high probability to reflect the situation of the real hQC protein structure. A first proof confirming this hypothesis can be found in the 10-fold higher measured potency of the corresponding 5-methylimidazoles as seen for the inhibitors **9** and **1**.

The evaluation of the biological efficacy of the presented hQC inhibitors was directed toward the ability of the suppression of the formation of $A\beta_{3(pE)-40,42}$ generated by the coexpressed hQC. The inhibitory potency of the compounds at the isolated target was found to be in good accordance with the activity of the compounds on the cellular level.

The presented study led to novel inhibitors of hQC with improved potency and activity in an in vitro cell system. For the first time a cell based system assessing the hQC inhibition potency in connection with the generation of $A\beta_{3(pE)-40,42}$ was used for the efficacy profiling. The results again emphasize the high probability of hQC to be the responsible enzyme for the cyclization of the N-terminal glutamate of $A\beta_{3,11(pE)-40,42}$ yielding $A\beta_{3(pE)-40,42}$ because the inhibitory potency and the efficacy in the cellular model were found to be in good correlation. The characterization of the most effective hQC inhibitors in transgenic animal models is currently underway.

Experimental Section

Chemistry. Starting materials and solvents were purchased from Aldrich and Maybridge Co. All chemical structures were confirmed by ^{1}H NMR and high-resolution mass spectrometry. The purity of the compounds was assessed by HPLC and confirmed to be ≥95%. The analytical HPLC system consisted of a Merck-Hitachi device (model LaChrom) utilizing a LiChrospher 100 RP 18 (5 μm), analytical column (length 125 mm, diameter 4 mm), and a diode array detector (DAD) with λ = 214 nm as the reporting wavelength. The compounds were analyzed using a gradient at a flow rate of 1 mL/min, where eluent A was acetonitrile and eluent B was water, both containing 0.1% (v/v) trifluoroacetic acid and applying the following gradient: method A, 0−min → 5% A, 5−17 min → 5−15% A, 15−27 min → 15−95% A, 27−30 min → 95% A; method B, 0−15 min → 5−50% A, 15−20 min → 50−95% A, 20−23 min → 95% A; method C, 0−20 min → 5−60% A, 20−25 min → 60−95% A, 25−30 min → 95% A. The purities of all reported compounds were determined by the percentage of the peak area at 214 nm. Semipreparative HPLC was performed on a Merck-Hitachi device (model LaChrom) equipped with a SP250/21 Nucleosil 100-7 C18 semipreparative column (Machery-Nagel). The compounds were eluted using the same solvent system as described above, applying a flow rate of 8 mL/min.

ESI mass spectra were obtained with a SCIEX API 365 spectrometer (Perkin-Elmer) utilizing the positive ionization mode. The high resolution positive ion ESI mass spectra were obtained from a Bruker Apex III 70e Fourier transform ion cyclotron resonance mass spectrometer (Bruker Daltonics, Billerica, MA) equipped with an Infinity cell, a 7.0 T superconducting magnet (Bruker, Karlsruhe, Germany), an rf-only hexapole ion guide, and an external electrospray ion source (API Apollo, voltages: end plate, −3.700 V; capillary, −4.400 V; capillary exit, 100 V; skimmer, 1.15 V; skimmer, 2.6 V). Nitrogen was used as drying gas at 150 °C. The sample solutions were introduced continuously via a syringe pump with a flow rate of 120 μL h^{-1}. All data were acquired with 256K data points and zero-filled to 1024K by averaging 32 scans.

The melting points were detected utilizing a Kofler melting point device and are not corrected. The ^{1}H NMR spectra were recorded at a Varian Gemini 2000 (400 MHz) or at a Bruker AC 500 (500 MHz) when 500 MHz is indicated. DMSO-d_6 was used unless otherwise specified. Chemical shifts are expressed as parts per million (ppm) downfield from tetramethylsilane. Splitting patterns have been designated as follows: s (singulet), d (doublet), dd (doublet of doublet), t (triplet), m (multiplet), and br (broad signal).

3-(5-Methyl-1*H*-imidazol-1-yl)propan-1-amine 6. Step A. 4-Methyl-1-trityl-1*H*-imidazole 3. 4-Methyl-1*H*-imidazole (36.53 mmol, 1 equiv) was dissolved in 120 mL of dimethylformamide, and triethylamine (73.06 mmol, 2 equiv) and chlorotriphenyl methane (40.1 mmol, 1.1 equiv) were added. The mixture was stirred for 3.5 h. The precipitate was filtered off and then washed by means of ice-cooled dimethylformamide (2 × 50 mL) and water (2 × 50 mL). After the solvent was removed, the remaining

product was dried over P_4O_{10}. Yield: 10.65 g (98.2%). The product was used without further purification.

Step B. 1-Trityl-3-[3-(1,3-dioxo-1,3-dihydro-2*H*-isoindol-2-yl)propyl]-1,4-dimethyl-1*H*-imidazol-3-ium Bromide 4. 4-Methyl-1-trityl-1*H*-imidazole (**3**) (32.85 mmol, 1 equiv) was suspended in acetonitrile (10 mL), and 2-(3-bromopropyl)isoindoline-1,3-dione (32.85 mmol, 1 equiv) was added. The mixture was kept under reflux overnight. The organic solvent was removed. Purification was achieved by flash chromatography using silica gel and a $CHCl_3$/MeOH gradient. Yield: 10.65 g (63.44%).

Step C. 2-(3-(5-Methyl-1*H*-imidazol-1-yl)propyl)isoindoline-1,3-dione 5. 1-Trityl-3-[3-(1,3-dioxo-1,3-dihydro-2*H*-isoindol-2-yl)-propyl]-1,4-dimethyl-1*H*-imidazol-3-ium bromide (**4**) (7.86 mmol) was dissolved in a stirred solution containing methanol (20 mL) and trifluoroacetic acid (4 mL). The mixture was kept under reflux overnight. The solvent was removed, and the remaining oil was purified by flash chromatography using silica gel and a $CHCl_3$/MeOH gradient. Yield: 2.05 g (97.0%).

Step D. 3-(5-Methyl-1*H*-imidazol-1-yl)propan-1-amine 6. 2-(3-(5-Methyl-1*H*-imidazol-1-yl)propyl)isoindoline-1,3-dione (**5**) (8.92 mmol, 1 equiv) and hydrazine monohydrate (17.84 mmol, 2 equiv) were dissolved in dry ethanol (50 mL). The mixture was kept under reflux overnight. Then this mixture was concentrated down to a volume of 25 mL. After that hydrochloric acid (concentrated, 55 mL) was added and the mixture was heated to 50 °C and kept at this temperature for 30 min. The formed precipitate was filtered off. The filtrate was cooled down to 0 °C, and solid NaOH was added until a final pH of 10−12 was reached. The aqueous solution was extracted by means of trichloromethane (3 × 50 mL). The combined organic layers were dried over Na_2SO_4 and filtered, and the solvent was removed. The product was purified by means of flash chromatography using silica gel and a $CHCl_3$/MeOH gradient. Yield: 0.74 g (60%). ^{1}H NMR (500 MHz, $CDCl_3$): δ 1.79−1.85 (m, 2H), 2.18 (s, 3H), 2.69−2.72 (m, 2H), 3.89−3.92 (m, 2H), 6.73 (s, H), 7.24 (s, solv), 7.38 (s, H). ESI-MS m/z: 140.3 $(M + H)^+$, 279.4 $(2M + H)^+$. HPLC (214 nm, method A): t_R dead time (100%).

3-(4-Methyl-1*H*-imidazol-1-yl)propan-1-amine 8. Step A. 2-(3-(4/5-Methyl-1*H*-imidazol-1-yl)propyl)isoindoline-1,3-dione. 4-Methyl-1*H*-imidazole (36.53 mmol, 1 equiv) and sodium hydride (60% in mineral oil, 36.53 mmol, 1.0 equiv) were dissolved in 80 mL of dimethylformamide. The mixture was stirred at room temperature for 2 h until the formation of hydrogen gas deceased. 2-(3-Bromopropyl)isoindoline-1,3-dione (34.70 mmol, 0.95 equiv) was added, and the mixture was stirred at 90 °C overnight. The solvent was removed, and the remaining residue was purified by means of flash chromatography using silica gel and a $CHCl_3$/MeOH gradient. Yield: 6.1 g (62.0%) of a mixture of 2-(3-(4-methyl-1*H*-imidazol-1-yl)propyl)isoindoline-1,3-dione and 2-(3-(5-methyl-1*H*-imidazol-1-yl)propyl)isoindoline-1,3-dione.

Step B. 2-(3-(4-Methyl-1*H*-imidazol-1-yl)propyl)isoindoline-1,3-dione 7. A mixture consisting of 2-(3-(4-methyl-1*H*-imidazol-1-yl)propyl)isoindoline-1,3-dione and 2-(3-(5-methyl-1*H*-imidazol-1-yl)propyl)isoindoline-1,3-dione (22.65 mmol, 1 equiv) and trityl chloride (13.6 mmol, 0.6 equiv) was dissolved in 40 mL of dichloromethane and kept at a temperature of 0 °C for 10 min and 1.5 h at room temperature. The solvent was removed, and the remaining solid was purified by means of flash chromatography using silica gel and a $CHCl_3$/MeOH gradient. Yield: 0.92 g (15.1%).

Step C. 3-(4-Methyl-1*H*-imidazol-1-yl)propan-1-amine 8. 2-(3-(4-Methyl-1*H*-imidazol-1-yl)propyl)isoindoline-1,3-dione (**7**) (3.42 mmol, 1 equiv) and hydrazine monohydrate (6.84 mmol, 2 equiv) were dissolved in 20 mL of ethanol, and the mixture was stirred for 12 h under reflux. The mixture was kept under reflux overnight and then concentrated to reach a volume of 25 mL. Hydrochloric acid (concentrated, 55 mL) was added, and the mixture was heated up to 50 °C and kept at this temperature for 30 min. The formed precipitate was filtered off. The filtrate was cooled down to 0 °C, and solid NaOH was added until a final pH of 10−12 was reached. The aqueous solution was extracted by means of $CHCl_3$ (3 × 50 mL). The combined organic layers were dried over Na_2SO_4 and filtered, and the solvent was removed. The product was purified by means of flash chromatography using silica gel and a $CHCl_3$/MeOH gradient containing aqueous ammonia (2% v/v). Yield: 0.31 g (65.1%). ^{1}H NMR (500 MHz, $CDCl_3$): δ 1.82−1.87 (m, 2H), 2.19 (s, 3H), 2.67−2.71 (m, 2H), 3.91−3.95 (m, 2H), 6.60 (s, H), 7.24 (s, solv.), 7.33 (s, H). ESI-MS m/z: 140.3 $(M + H)^+$, 279.4 $(2M + H)^+$. HPLC (214 nm, method A): t_R = 0.2 min (100%).

Synthesis of the Compounds 9−12. The synthesis was accomplished as previously described.[26]

General Procedure for the Synthesis of the Cyanoguanidines 13−21, 36−40, 51. All reactions were performed at a Buchi Synchor parallel synthesizer. A typical reaction mixture consisted of sodium cyanamide (0.26 g, 4.0 mmol, 1 equiv), and the corresponding isothiocyanate (4.0 mmol, 1.0 equiv) was dissolved in 10 mL of ethanol. The mixture was shaken for 3 h under reflux and then cooled to room temperature. Either 3-(1*H*-imidazol-1-yl)propyl-1-amine, 3-(5-methyl-1*H*-imidazol-1-yl)propyl-1-amine (**6**), or 3-(4-methyl-1*H*-imidazol-1-yl)propyl-1-amine (**8**) (each, 4.8 mmol, 1.2 equiv) and *N*1-((ethylimino)methylen)-*N*3,*N*3-dimethylpropan-1,3-diamin-hydrochloride (WSCD, 0.92 g, 4.8 mmol, 1 equiv) and dimethylformamide (5 mL) were added. The mixture was shaken for 3 h at room temperature, and after that the organic solvent was removed. The remaining oil was dissolved in trichloromethane (30 mL), and the organic layer was washed once with water (20 mL), dried over Na_2SO_4, and filtered off, and the solvent was removed. Purification was performed by applying flash chromatography on basic aluminum oxide using a $CHCl_3$/MeOH gradient.

General Procedure for the Synthesis of the Nitrovinyldiamines 22−30, 41−45, 52. A typical reaction batch consisted of 1,1-bis(methylthio)-2-nitroethene (0.70 g, 4.2 mmol, 1 equiv) and the corresponding primary amine (4.0 mmol, 1 equiv) dissolved in ethanol (20 mL). The mixture was stirred for 24 h under reflux. 3-(1*H*-Imidazol-1-yl)propyl-1-amine or 3-(5-methyl-1*H*-imidazol-1-yl)propyl-1-amine (**6**) or 3-(4-methyl-1*H*-imidazol-1-yl)propyl-1-amine (**8**) (each, 4.2 mmol, 1 equiv) was added, and the mixture was stirred for 24 h under reflux. The solvent was removed, and the resulting oils were purified by means of flash chromatography using silica gel as the solid phase and a $CHCl_3$/MeOH gradient.

General Procedure for the Synthesis of 2-Thioxopyrimidine-4(1*H*)-ones 31−35, 46−50, 53. A typical reaction batch consisted of 3-(1*H*-imidazol-1-yl)propan-1-amine (4.0 mmol, 1 equiv) or **6** or **8** (each, 1.43 mmol, 1 equiv), and the corresponding isothiocyanate (1 equiv) was dissolved in dry ethanol (20 mL) and heated under reflux for 3 h. After the solvent was removed the products were purified by means of flash chromatography using silica gel and a $CHCl_3$/MeOH gradient.

Inhibitor Testing. QC activity was evaluated fluorometrically in a coupled assay according to the method previously described.[44] Gln-AMC served as substrate and pyroglutamyl peptidase as auxiliary enzyme. After conversion of Gln-AMC into pGlu-AMC by QC the pGlu-AMC was hydrolyzed by pyroglutamyl peptidase (pGAP). The generated AMC was detected with excitation/emission wavelengths of 380/460 nm. The described assay was modified as follows for the use in a higher throughput:

The used buffer consisted of 50 mM Tris-HCl (ROTH, Karlsruhe, Germany), with pH 8.0, adjusted with HCl. The substrate H-Gln-AMC hydrobromide (AMC: 7-amido-4-methylcoumarin; BACHEM, Bubendorf, Switzerland) was used in a concentration of 0.625 mM. The auxiliary enzyme pGAP from *Bacillus amyloliquefaciens* (10 units, 25 units/mL;

Qiagen, Hilden, Germany) was prediluted 1:10 in Tris-HCl. Human glutaminyl cyclase (QC, EC 2.3.2.5) was recombinantly expressed in *Pichia pastoris* and purified as previously described.[45] The protein concentration was adjusted to be 0.6 mg/mL, and the hQC solution was prediluted to 1:1250 in Tris-HCl. A typical reaction mixture consisted of 100 μL of substrate, 100 μL of the inhibitor (stock solution in DMSO), resulting in a final DMSO concentration of 5%, and 25 μL of pGAP. After incubation in NUNC 96 flat bottom transparent microwell plates (Nunc, Roskilde, Denmark) for 10 min at 30 °C the reaction was started by adding 25 μL of the hQC solution. All enzyme activity measurements were performed in triplicate. A GENios Pro multifunctional microwell plate photometer working on Magellan software, version 4.0 (top and bottom reading, TECAN, Switzerland), was used to monitor the progress curves for 20 min at 30 °C. Pipetting steps were accomplished using a Tecan Genesis Freedom 200 workstation (Gemini software, version 4.0; TECAN, Switzerland). The kinetic data were evaluated using GraFit (version 5.0.4, Erithacus, Horley, U.K.).

Cell Based Assay. The inhibition of $A\beta_{3(pE)-40,42}$ formation was evaluated in HEK293 cells overexpressing mutated human amyloid precursor protein APP(NLE) and human glutaminyl cyclase (hQC)[35] according to the following protocol: Human embryonic kidney cells HEK293 were cultured in DMEM (10% FBS) (Invitrogen) in a humidified atmosphere of 5% CO_2 at 37 °C. Then 250 000 cells/500 μL were seeded per well in a 24-well plate. After 24 h the cells were transfected with 0.8 μg of APP-NLE vector, 0.8 μg of hQC vector, and 4 μL of Lipofectamine 2000 (Invitrogen) in 100 μL of OPTIMEM for 5 h. The cells were further cultivated in the DMEM medium. The next day, cells were incubated in the assay medium (DMEM, without phenol red, without FBS) containing an appropriate amount of QC inhibitor or control. The inhibitor stock solution (10 mM) was therefore diluted stepwise with DMSO (Sigma-Aldrich, Taufkirchen, Germany) and medium. The final DMSO concentration was 0.01%. The inhibitor concentration in the medium was 1 μM using five replicates. After 24 h of the inhibitor application the supernatant (250 μL) was collected and readily mixed with 25 μL of complete mini protease inhibitor cocktail (Roche, Basel, Switzerland) supplemented in addition with 10 mM AEBSF (Roth, Karlsruhe, Germany). After centrifugation (2000*g* for 5 min) 2 aliquots (120 μL) of supernatant were collected and the total $A\beta_{X-40,42}$ and $A\beta_{3(pE)-40,42}$ concentrations were determined using specific sandwich ELISAs (IBL, Hamburg, Germany) according to the manufacturers advices.

Computational Chemistry. All calculations were performed using the software packages MOE, version 2007.08 (CCG, Montreal, Canada); GOLD, version 4.0 (CCDC Software Ltd., Cambridge, U.K.); SYBYL, verssion 8.0 (Tripos CL, St. Louis, MO); ProSa2003, version 4.0 (CAME, Salzburg, Austria);[46,47] PROCHECK, version 3.5.4 (European Bioinformatics Institute, Cambridge, U.K.)[48] on a 9 CPU computer cluster with CentOS 4.6 operation system installed.

hQC Homology Model. The Charmm22 force field (MOE, version 2007.08) was set as default for all modeling steps, if not mentioned otherwise. The implicit general Born solvation[49] was turned on in all MD simulations (Supporting Information).

Docking. The imidazole residue of the inhibitor **1** obtained from the homology model was used as a scaffold constraint. All docking runs were performed 20 times for each molecule not allowing early termination using the ChemScore as the scoring function implemented in the software GOLD. The best-ranking poses were used for further analysis of the docking solutions (Supporting Information).

Acknowledgment. The authors thank Dr. F. Rosche and Dr. R. Wolf for providing the ESI-MS spectra and Dr. J. Schmidt from the Leibniz Institute of Plant Biochemistry, Halle, Germany, for recording the high resolution mass spectra. The authors are also grateful to M. Scharfe and H. Mosdzen for technical support. This work was supported by The Federal Ministry of Education and Research, Germany, Grant Nos. 0313185 and 0315089 (to H.-U.D.).

Supporting Information Available: Detailed analytical data of the compounds (NMR, MS, high resolution MS, HPLC), yields, description of the homology model development including the model characteristic data, and fitness and scoring results of the docking experiments. This material is available free of charge via the Internet at http://pubs.acs.org.

References

(1) Awade, A. C.; Cleuziat, P.; Gonzales, T.; Robert-Baudouy, J. Pyrrolidone carboxyl peptidase (Pcp): an enzyme that removes pyroglutamic acid (pGlu) from pGlu-peptides and pGlu-proteins. *Proteins* **1994**, *20*, 34–51.
(2) Abraham, G. N.; Podell, D. N. Pyroglutamic acid. Non-metabolic formation, function in proteins and peptides, and characteristics of the enzymes effecting its removal. *Mol. Cell. Biochem.* **1981**, *38*, 181–190.
(3) Van Coillie, E.; Proost, P.; Van, A., I; Struyf, S.; Polfliet, M.; De, M., I; Harvey, D. J.; Van Damme, J.; Opdenakker, G. Functional comparison of two human monocyte chemotactic protein-2 isoforms, role of the amino-terminal pyroglutamic acid and processing by CD26/dipeptidyl peptidase IV. *Biochemistry* **1998**, *37*, 12672–12680.
(4) Busby, W. H.; Humm, J.; Kizer, J. S.; Youngblood, W. W.; Quackenbush, G. An enzyme(s) that converts glutaminyl-peptides into pyroglutamyl-peptides. Presence in pituitary, brain, adrenal medulla, and lymphocytes. *J. Biol. Chem.* **1987**, *262*, 8532–8536.
(5) Messer, M.; Ottesen, M. Isolation and properties of glutamine cyclotransferase of dried papaya latex. *Biochim. Biophys. Acta* **1964**, *92*, 409–411.
(6) Fischer, W. H.; Spiess, J. Identification of a mammalian glutaminyl cyclase converting glutaminyl into pyroglutamyl peptides. *Proc. Natl. Acad. Sci. U.S.A.* **1987**, *84*, 3628–3632.
(7) Pohl, T.; Zimmer, M.; Mugele, K.; Spiess, J. Primary structure and functional expression of a glutaminyl cyclase. *Proc. Natl. Acad. Sci. U.S.A.* **1991**, *88*, 10059–10063.
(8) Fraser, L. R. Fertilization promoting peptide: an important regulator of sperm function in vivo? *Rev. Reprod.* **1998**, *3*, 151–154.
(9) Schilling, S.; Niestroj, A. J.; Rahfeld, J. U.; Hoffmann, T.; Wermann, M.; Zunkel, K.; Wasternack, C.; Demuth, H.-U. Identification of human glutaminyl cyclase as a metalloenzyme. Potent inhibition by imidazole derivatives and heterocyclic chelators. *J. Biol. Chem.* **2003**, *278*, 49773–49779.
(10) Bateman, R. C., Jr.; Temple, J. S.; Misquitta, S. A.; Booth, R. E. Evidence for essential histidines in human pituitary glutaminyl cyclase. *Biochemistry* **2001**, *40*, 11246–11250.
(11) Schilling, S.; Manhart, S.; Hoffmann, T.; Ludwig, H.-H.; Wasternack, C.; Demuth, H.-U. Substrate specifity of glutaminyl cyclases from plants and animals. *Biol. Chem.* **2003**, *384*, 1583–1592.
(12) Booth, R. E.; Lovell, S. C.; Misquitta, S. A.; Bateman, R. C., Jr. Human glutaminyl cyclase and bacterial zinc aminopeptidase share a common fold and active site. *BMC Biol.* **2004**, *2*, 2.
(13) Huang, K. F.; Liu, Y. L.; Cheng, W. J.; Ko, T. P.; Wang, A. H. Crystal structures of human glutaminyl cyclase, an enzyme responsible for protein N-terminal pyroglutamate formation. *Proc. Natl. Acad. Sci. U.S.A.* **2005**, *102*, 13117–13122.
(14) Huang, K. F.; Liu, Y. L.; Wang, A. H. Cloning, expression, characterization, and crystallization of a glutaminyl cyclase from human bone marrow: a single zinc metalloenzyme. *Protein Expression Purif.* **2005**, *43*, 65–72.
(15) Song, I.; Temple, J. S.; Burns, K. H.; Bateman, R. C., Jr. Absence of an essential thiol in human glutaminyl cyclase: implications for mechanism. *Korean J. Biol. Sci.* **1998**, *2*, 243–248.
(16) Cynis, H.; Rahfeld, J. U.; Stephan, A.; Kehlen, A.; Koch, B.; Wermann, M.; Demuth, H.-U.; Schilling, S. Isolation of an isoenzyme of human glutaminyl cyclase: retention in the Golgi complex suggests involvement in the protein maturation machinery. *J. Mol. Biol.* **2008**, *379*, 966–980.
(17) Bockers, T. M.; Kreutz, M. R.; Pohl, T. Glutaminyl-cyclase expression in the bovine/porcine hypothalamus and pituitary. *J. Neuroendocrinol.* **1995**, *7*, 445–453.
(18) Saido, T. C.; Iwatsubo, T.; Mann, D. M.; Shimada, H.; Ihara, Y.; Kawashima, S. Dominant and differential deposition of distinct

beta-amyloid peptide species, A beta N3(pE), in senile plaques. *Neuron* **1995**, *14*, 457–466.
(19) Schilling, S.; Zeitschel, U.; Hoffmann, T.; Heiser, U.; Francke, M.; Kehlen, A.; Holzer, M.; Hutter-Paier, B.; Prokesch, M.; Windisch, M.; Jagla, W.; Schlenzig, D.; Lindner, C.; Rudolph, T.; Reuter, G.; Cynis, H.; Montag, D.; Demuth, H.-U.; Rossner, S. Glutaminyl cyclase inhibition attenuates pyroglutamate Abeta and Alzheimer's disease-like pathology. *Nat. Med.* **2008**, *14*, 1106–1111.
(20) Miravalle, L.; Calero, M.; Takao, M.; Roher, A. E.; Ghetti, B.; Vidal, R. Amino-terminally truncated Abeta peptide species are the main component of cotton wool plaques. *Biochemistry* **2005**, *44*, 10810–10821.
(21) Schilling, S.; Hoffmann, T.; Manhart, S.; Hoffmann, M.; Demuth, H.-U. Glutaminyl cyclases unfold glutamyl cyclase activity under mild acid conditions. *FEBS Lett.* **2004**, *563*, 191–196.
(22) Schilling, S.; Lauber, T.; Schaupp, M.; Manhart, S.; Scheel, E.; Bohm, G.; Demuth, H.-U. On the seeding and oligomerization of pGlu-amyloid peptides (in vitro). *Biochemistry* **2006**, *45*, 12393–12399.
(23) Youssef, I.; Florent-Bechard, S.; Malaplate-Armand, C.; Koziel, V.; Bihain, B.; Olivier, J. L.; Leininger-Muller, B.; Kriem, B.; Oster, T.; Pillot, T. N-Truncated amyloid-beta oligomers induce learning impairment and neuronal apoptosis. *Neurobiol. Aging* **2007**, *29*, 1319–1333.
(24) Russo, C.; Violani, E.; Salis, S.; Venezia, V.; Dolcini, V.; Damonte, G.; Benatti, U.; D'Arrigo, C.; Patrone, E.; Carlo, P.; Schettini, G. Pyroglutamate-modified amyloid beta-peptides—AbetaN3(pE)—strongly affect cultured neuron and astrocyte survival. *J. Neurochem.* **2002**, *82*, 1480–1489.
(25) Schilling, S.; Appl, T.; Hoffmann, T.; Cynis, H.; Schulz, K.; Jagla, W.; Friedrich, D.; Wermann, M.; Buchholz, M.; Heiser, U.; von Horsten, S.; Demuth, H.-U. Inhibition of glutaminyl cyclase prevents pGlu-Abeta formation after intracortical/hippocampal microinjection in vivo/in situ. *J. Neurochem.* **2008**, *106*, 1225–1236.
(26) Buchholz, M.; Heiser, U.; Schilling, S.; Niestroj, A. J.; Zunkel, K.; Demuth, H.-U. The first potent inhibitors for human glutaminyl cyclase: synthesis and structure−activity relationship. *J. Med. Chem.* **2006**, *49*, 664–677.
(27) Thornber, C. W. Isosterism and molecular modification in drug design. *Chem. Soc. Rev.* **1979**, *8*, 563–580.
(28) Patani, G. A.; LaVoie, E. J. Bioisosterism: a rational approach in drug design. *Chem. Rev.* **1996**, *96*, 3147–3176.
(29) Lima, L. M.; Barreiro, E. J. Bioisosterism: a useful strategy for molecular modification and drug design. *Curr. Med. Chem.* **2005**, *12*, 23–49.
(30) Durant, G. J.; Emmett, J. C.; Ganellin, C. R.; Miles, P. D.; Parsons, M. E.; Prain, H. D.; White, G. R. Cyanoguanidine-thiourea equivalence in the development of the histamine H2-receptor antagonist, cimetidine. *J. Med. Chem.* **1977**, *20*, 901–906.
(31) Duncan, W. A.; Parsons, M. E. Reminiscences of the development of cimetidine. *Gastroenterology* **1980**, *78*, 620–625.
(32) Atwal, K. S.; Ahmed, S. Z.; O'Reilly, B. C. A facile synthesis of cyanoguanidines from thioureas. *Tetrahedron Lett.* **1989**, *30*, 7313–7316.
(33) Stankovic, S.; Skobaljic, N.; Stojanovic, N.; Stojicic, S. Procedure for Synthesis of *N*-[2[[[5-[(Dialkylamino)methyl]-2-furanyl]-methyl]thyo]ethyl]-*N*′-alkyl-2-nitro-1,1-alkenediamines and Their Hydrochlorides. PCT/YU99/00011, **2000**; pp 1−11.
(34) Shirotani, K.; Tsubuki, S.; Lee, H. J.; Maruyama, K.; Saido, T. C. Generation of amyloid beta peptide with pyroglutamate at position 3 in primary cortical neurons. *Neurosci. Lett.* **2002**, *327*, 25–28.
(35) Cynis, H.; Scheel, E.; Saido, T. C.; Schilling, S.; Demuth, H.-U. Amyloidogenic processing of amyloid precursor protein: evidence of a pivotal role of glutaminyl cyclase in generation of pyroglutamate-modified amyloid-beta. *Biochemistry* **2008**, *47*, 7405–7413.
(36) Henikoff, S.; Henikoff, J. G. Amino acid substitution matrices from protein blocks. *Proc. Natl. Acad. Sci. U.S.A.* **1992**, *89*, 10915–10919.
(37) Schilling, S.; Cynis, H.; von Bohlen, A.; Hoffmann, T.; Wermann, M.; Heiser, U.; Buchholz, M.; Zunkel, K.; Demuth, H.-U. Isolation, catalytic properties, and competitive inhibitors of the zinc-dependent murine glutaminyl cyclase. *Biochemistry* **2005**, *44*, 13415–13424.
(38) Prescott, J. M.; Wagner, F. W.; Holmquist, B.; Vallee, B. L. Spectral and kinetic studies of metal-substituted Aeromonas aminopeptidase: nonidentical, interacting metal-binding sites. *Biochemistry* **1985**, *24*, 5350–5356.
(39) Bayliss, M. E.; Prescott, J. M. Modified activity of Aeromonas aminopeptidase: metal ion substitutions and role of substrates. *Biochemistry* **1986**, *25*, 8113–8117.
(40) Chevrier, B.; Schalk, C.; D'Orchymont, H.; Rondeau, J. M.; Moras, D.; Tarnus, C. Crystal structure of *Aeromonas proteolytica* aminopeptidase: a prototypical member of the co-catalytic zinc enzyme family. *Structure* **1994**, *2*, 283–291.
(41) Cole, J. C.; Nissink, W. M.; Taylor, R. Protein−Ligand Docking and Virtual Screening with GOLD. In *Virtual Screening in Drug Discovery*; Alvarez, J., Shoichet, S., Eds.; Taylor & Francis: Boca Raton, FL, 2005; pp 379−415.
(42) Ajay; Murcko, M. A. Computational methods to predict binding free energy in ligand−receptor complexes. *J. Med. Chem.* **1995**, *38*, 4953–4967.
(43) Szegezdi, J.; Csizmadia, F. A Method for Calculating the pK_a Values of Small and Large Molecules. http://www.chemaxon.com/conf/Calculating_pKa_values_of_small_and_large_molecules.pdf (**2009**); ChemAxon.
(44) Schilling, S.; Hoffmann, T.; Wermann, M.; Heiser, U.; Wasternack, C.; Demuth, H.-U. Continuous spectrometric assays for glutaminyl cyclase activity. *Anal. Biochem.* **2002**, *303*, 49–56.
(45) Schilling, S.; Hoffmann, T.; Rosche, F.; Manhart, S.; Wasternack, C.; Demuth, H.-U. Heterologous expression and characterization of human glutaminyl cyclase: evidence for a disulfide bond with importance for catalytic activity. *Biochemistry* **2002**, *41*, 10849–10857.
(46) Sippl, M. J. Recognition of errors in three-dimensional structures of proteins. *Proteins* **1993**, *17*, 355–362.
(47) Hendlich, M.; Lackner, P.; Weitckus, S.; Floeckner, H.; Froschauer, R.; Gottsbacher, K.; Casari, G.; Sippl, M. J. Identification of native protein folds amongst a large number of incorrect models. The calculation of low energy conformations from potentials of mean force. *J. Mol. Biol.* **1990**, *216*, 167–180.
(48) Laskowski, R. A.; MacArthur, M. W.; Moss, D. S.; Thornton, J. M. PROCHECK: a program to check the stereochemical quality of protein structures. *J. Appl. Crystallogr.* **1993**, *26*, 283–291.
(49) Pellegrini, E.; Field, M. J. A generalized-Born solvation model for macromolecular hybrid-potential calculations. *J. Phys. Chem. A* **2002**, *106*, 1316–1326.